Bowhead whale localization using asynchronous hydrophones in the Chukchi Sea

Graham A. Warner,[1,a)] Stan E. Dosso,[1] David E. Hannay,[2] and Jan Dettmer[1]
[1]*School of Earth and Ocean Sciences, University of Victoria, 3800 Finnerty Road, Suite 405A, Victoria, British Columbia V8P 5C2, Canada*
[2]*JASCO Applied Sciences, 2305-4464 Markham Street, Victoria, British Columbia V8Z 7X8, Canada*

(Received 14 January 2016; revised 6 May 2016; accepted 6 June 2016; published online 5 July 2016)

This paper estimates bowhead whale locations and uncertainties using non-linear Bayesian inversion of their modally-dispersed calls recorded on asynchronous recorders in the Chukchi Sea, Alaska. Bowhead calls were recorded on a cluster of 7 asynchronous ocean-bottom hydrophones that were separated by 0.5–9.2 km. A warping time-frequency analysis is used to extract relative mode arrival times as a function of frequency for nine frequency-modulated whale calls that dispersed in the shallow water environment. Each call was recorded on multiple hydrophones and the mode arrival times are inverted for: the whale location in the horizontal plane, source instantaneous frequency (IF), water sound-speed profile, seabed geoacoustic parameters, relative recorder clock drifts, and residual error standard deviations, all with estimated uncertainties. A simulation study shows that accurate prior environmental knowledge is not required for accurate localization as long as the inversion treats the environment as unknown. Joint inversion of multiple recorded calls is shown to substantially reduce uncertainties in location, source IF, and relative clock drift. Whale location uncertainties are estimated to be 30–160 m and relative clock drift uncertainties are 3–26 ms. © *2016 Acoustical Society of America*. [http://dx.doi.org/10.1121/1.4954755]

[AMT] Pages: 20–34

I. INTRODUCTION

Acoustic localization of vocalizing marine mammals is important for characterizing their spatial distributions, movement behaviors and grouping, and for source level measurements. This paper develops a Bayesian approach to localize bowhead whales in the Chukchi Sea based on modal dispersion of their calls, including a quantitative uncertainty analysis that accounts for unknown environmental parameters, call source signal, and recorder clock drifts. Several studies have employed localization methods to examine bowhead whale movement and behavior changes in the Chukchi and Beaufort Seas due to exposures to anthropogenic underwater noise, mainly associated with offshore oil and gas exploration activities.[1,2]

The western arctic bowhead whale population migrates annually between wintering areas in the Bering Sea and summer feeding areas off the Mackenzie Delta in the Beaufort Sea. Their fall migration occurs from September through November along the Beaufort coast and through the central northeastern Chukchi Sea.[3–5]

Oil and gas exploration and increased shipping has occurred spatially and temporally coincident with bowhead summer feeding and fall migration. There is concern that anthropogenic noise from these activities could affect the whale's use of sounds for critical life functions such as navigating, avoiding predators, and maintaining group structure. A recent study has found bowheads modify their calling behavior in the presence of quite low levels of seismic survey noise.[6] There is further concern that anthropogenic noise exposures during or prior to subsistence whale hunting could modify bowhead swimming behaviors, potentially making the hunts more difficult;[7] however, the relationship between noise exposure and effects is poorly understood.

A common strategy to reduce marine mammal exposures to anthropogenic noise is to carry out anthropogenic activities during times when animals are not present and at locations away from high animal densities. This approach requires knowledge of the temporal and spatial distributions of animals. Passive acoustic monitoring, based on listening for natural sounds produced by animals, is an increasingly popular method for measuring temporal and spatial distributions that causes no disturbance to the animals.

Bowhead whales make a variety of sounds including frequency-modulated (FM) sweeps, moans, amplitude-modulated pulsive calls, and songs.[5,8] During the fall migration, most bowhead calls are moans and low frequency (<400 Hz) FM sweeps. Recordings of these calls can be used to localize the whales.

Several approaches have been developed for localizing whales using low-frequency calls. Distributions of directional autonomous seafloor acoustic recorders (DASARs) have been used in the Beaufort Sea to triangulate whale locations using the bearing estimates from multiple recorders.[9–11] Clark and Ellison[12] used a linear omni-directional (time-synchronized) hydrophone array deployed along an ice ridge to estimate whale locations from call arrival time differences. Several studies have used (synchronized) vertical line arrays to exploit sound propagation effects for low-frequency calls in shallow

a)Electronic mail: gwarner@uvic.ca

water.[11,13,14] These studies used normal-mode propagation in a variety of ways (e.g., matched-field and matched-mode processing) to estimate source locations. Sei whales, which also make low-frequency calls, have been tracked in three dimensions by using normal-mode models to back-propagate calls recorded on synchronized horizontal and vertical arrays.[15]

There has been some effort to obtain range estimates for whales using a single hydrophone because of the relative simplicity and low cost of the equipment required. In particular, range estimation based on low-frequency right whale and bowhead whale calls has been achieved by exploiting the frequency-dependence of acoustic normal mode group speeds in shallow water environments.[16,17] In shallow water, the environment supports a limited number of propagating modes, each of which supports a continuum of frequencies. The frequency- and mode-dependence of modal group speeds (which we collectively refer to as *modal dispersion* in this paper) is well modeled with normal-mode theory.[18] Signals disperse as they propagate, with higher frequencies generally traveling faster than lower frequencies within a mode, and higher-order modes generally traveling slower than lower-order modes for a given frequency. This frequency-dependence affects mode arrival times in proportion to the source-receiver range (within the range-independent assumption) so dispersion measurements can be made by analyzing signals recorded at a single hydrophone using time-frequency (TF) methods. However, modal arrival times also depend on environmental properties [e.g., water-column sound-speed profile (SSP) and seabed geoacoustic parameters] and on the TF characteristics of the acoustic signal emitted by the source [the instantaneous frequency[19] (IF) function], which are usually not well known in marine mammal applications, complicating localization. Resolving mode arrival times in the TF plane requires sufficient signal bandwidth and is also dependent on the difference in modal group speeds and the signal processing techniques applied. For relatively short-duration FM calls received at long ranges, modes are well separated in time and arrival times can be determined from the magnitude of a short-time Fourier transform (STFT). At close ranges, mode arrivals are difficult to separate in the TF plane. Mode-warping techniques used to improve the TF resolution of modes for close-range dispersion measurements of impulsive sounds[20] have recently been modified and successfully applied to FM bowhead calls.[17] This paper applies the modified mode-warping technique to FM calls or portions of calls that monotonically increase or decrease in frequency with time.

The single-hydrophone range-estimation studies using normal-mode theory[16,17] parameterized the acoustic environment with a range-independent model consisting of a water layer over a fluid half-space. Wiggins *et al.*[16] fixed environmental parameter values using historical information and assessed sensitivity of modal group speeds by varying the mean water sound speed and seafloor sound speed independently for a few parameter perturbations. Bonnel *et al.*[17] used a Pekeris waveguide with fixed water sound speed from conductivity-temperature-depth measurements and varied the seafloor sound speed over a discretized interval. In that study, the bathymetry was strongly range-dependent; however, independent DASAR measurements showed the single-hydrophone range estimates were reasonably accurate despite the violation of the range-independent assumption. It is difficult to assess the uncertainty of range estimates using these approaches in general without additional information because the fixed environmental parameterization (e.g., Pekeris waveguide) and constrained parameter values may not provide an appropriate level of model complexity that corresponds to the information content of the data. Hence, these approaches could under-parameterize the environmental model which could, in turn, lead to underestimation of range uncertainty.

This paper estimates bowhead whale locations and their uncertainties in the horizontal plane from the dispersion of normal modes recorded with multiple non-synchronized omni-directional hydrophones in a shallow-water (approximately) range-independent environment. We use a general model for the unknown environment to rigorously quantify its effect on localization uncertainties. In particular, a trans-dimensional (trans-D) Bayesian inversion approach is applied for the water SSP and for the sub-bottom to allow the data to estimate how much environmental structure is appropriate.[21] The SSP has a $1/c_w^2$ piecewise-linear gradient (c_w is water sound speed) defined by an unknown number of depth/sound-speed nodes. The sub-bottom consists of an unknown number of homogeneous sediment layers, each having unknown thickness, sound speed, and density, overlying a half-space. The trans-D algorithm samples over the number of SSP nodes and sub-bottom layers and their parameter values so the range estimates and their uncertainties account for realistic environmental uncertainty.

A standard time-difference-of-arrival localization approach is not applicable here because the recorders were not synchronized due to clock drift after deployment. Using arrival time differences between modes from multiple asynchronous recorders could be used as data in a combined localization/environmental inversion (often referred to as focalization), but this ignores information contained in calls or portions of calls that have only one detectable mode. Utilizing this information requires treating as unknowns the source IF (a function of frequency to be estimated) and the relative recorder clock drifts, and inverting arrival times (as opposed to arrival time differences). While this approach involves more unknown parameters, it allows more data information to be used, providing whale locations based on recorded calls composed of as few as one detectable mode. We use this approach to invert the modal arrival times measured at each recorder relative to a reference recorder clock. Range information in the data for multiple distributed recorders constrains the whale location in the horizontal plane. The data also constrain the relative clock drifts, providing information to synchronize the recorders. We apply the new algorithm to single and multiple whale calls and show that localization and synchronization results are significantly improved if arrival times from multiple calls are inverted jointly. The Bayesian inversion developed here estimates parameter values and uncertainties for whale location, source IF, water SSP (including effective water depth), sub-bottom layering and geoacoustic parameters, relative recorder clock drift (synchronization), and residual error

statistics. To our knowledge, whale localization based on inversion of modal dispersion of FM whale calls from asynchronous recorders has not been reported previously. This method can be applied to data collected by relatively inexpensive recorders that are easy to deploy (compared to synchronized hydrophone arrays or directional sensors).

This method is limited to shallow water, range-independent environments, with low-frequency FM calls that disperse as they propagate. The source-receiver range has to be large enough such that mode dispersion is quantifiable (the minimum range is generally dependent on the TF characteristics of the call and the environmental properties) but not so large that range-dependent effects violate the range-independent approximation. Mode amplitudes are not required except in the sense that they must be higher than background noise such that accurate mode arrival times can be determined. We applied a threshold of approximately 5 dB for this paper.

Whale depth is not required or estimated using this approach; however, a whale calling at the depth of a mode-function node will not excite that mode. In general, a missing mode will not necessarily preclude successful localization, particularly in multi-call inversions. However, if a missing mode leads to misidentification of the mode (e.g., mode 3 is identified as mode 2), the localization will likely fail. Applying the inversion to multiple whale calls may increase the robustness if the call depths differ, as wrongly-identified mode arrivals would likely be fit poorly and could be reassigned in a subsequent inversion.

The trans-D Bayesian inversion is applied to acoustic data collected from August to October 2013 using seven autonomous ocean-bottom hydrophone (OBH) recorders which were part of an underwater sound measurement program in the Chukchi Sea, Alaska.[22] The program was originally designed to determine ambient noise levels, quantify sound levels from oil and gas exploration activities, and investigate spatial and temporal distributions of marine mammals based on their calls. The seven OBHs recorded thousands of bowhead whale calls including low-frequency FM sweeps. Many of these sweeps showed significant dispersion in the TF plane and were recorded on multiple OBHs. In this paper we apply the Bayesian focalization algorithm in a simulation study to investigate the impact of varying degrees of environmental knowledge on localization and then to 9 bowhead whale calls recorded within 3.25 min on multiple OBHs.

II. THEORY

A. Data processing

Bowhead whale calls include low-frequency moans and sweeps that can excite several propagating modes in shallow waters, which can be modeled using normal-mode theory.[18] Modes propagate with different group speeds that are dependent on the environment, i.e., the water-column SSP and geoacoustic properties of the sub-bottom. At long ranges, mode arrivals (for a fixed frequency) are well separated in time and can be determined from the TF representations of a recorded call. A recent study used a mode warping technique to improve the modal TF resolution of non-impulsive bowhead whale calls[17] based on a similar technique used previously for impulsive sounds.[20] To apply mode warping to non-impulsive signals,[17] the received signal is first deconvolved with an approximate (empirical) source IF designed to decrease the received signal duration for subsequent mode warping. In practice the empirical source IF is manually estimated by an IF function that has a shape that is similar to, but precedes, the mode 1 arrival. The deconvolved signal is then warped using standard methods and transformed into the warped-TF domain using a STFT. Each mode is filtered in the warped-TF domain, transformed back into the warped-time domain using an inverse STFT, unwarped into the original time domain using standard methods, and transformed into the TF domain with a STFT. The mode arrival times (picks) are determined from the time of maximum energy of the deconvolved filtered mode in the TF domain and then corrected using the empirical source IF. The inversion is not sensitive to the empirical source IF because of this correction. For impulsive sounds in an approximately range-independent waveguide, warping transforms the dispersed modes into near-constant frequency tones that can be band-pass filtered to separate the modes. For frequency sweeps, deconvolution and warping separates the modes, but it is often difficult to achieve sufficient separation such that a band-pass filter isolates individual modes. Hence, warped modes are filtered using a TF mask (a manually defined polygon in TF space) and transformed back into the time domain using an inverse STFT. This process improves the accuracy of estimated mode arrival times and extends the bandwidth over which modes are resolved. Figure 1 illustrates the data processing procedure for a bowhead whale call recorded in the Chukchi Sea (described further in Sec. IV).

For each filtered mode, a spectrogram (magnitude of STFT) is computed using a Hanning window with 99% overlap (Fig. 1 considers a 16 384-point window for data sampled at 64 kHz). The mode arrival time data are limited to frequencies where mode arrivals have high enough levels such that the arrival times are not significantly influenced by background noise. In practice this can be difficult to determine *a priori*; however, poor data can often be identified by performing a preliminary inversion to detect outliers (i.e., data residuals that lie several standard deviations outside of the assumed Gaussian distribution). Those data can then be discarded and the inversion rerun on the reduced dataset.

B. Bayesian inversion

The mode arrival-time picks indicated in Fig. 1(a) are dependent on the whale location, source IF, environment, and relative recorder clock drifts. The arrival time of mode m at frequency f for whale call w at recorder a is

$$t_{wam}(f) = \tau_w(f) + \frac{\sqrt{(x_w - X_a)^2 + (y_w - Y_a)^2}}{v_m(\mathbf{e}, f)} + \Delta_a, \quad (1)$$

where $\tau_w(f)$ is the source IF [i.e., $\tau_w(f)$ is the time that frequency f was emitted by whale w], x_w and y_w are the easting and northing coordinates of the whale, X_a and Y_a are the

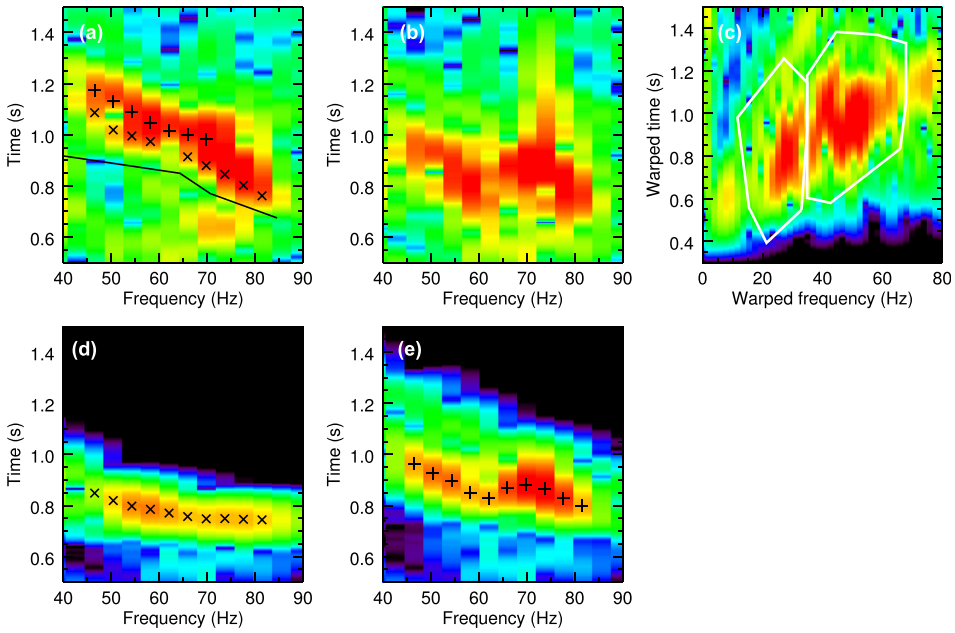

FIG. 1. (Color online) Example of warping TF analysis. (a) Recorded bowhead whale call spectrogram and empirical source IF (solid line). (b) Spectrogram after deconvolution by source IF. (c) Warped spectrogram showing two modes and the inverse TF masks (white polygons). (d) and (e) Filtered spectrograms with deconvolved data picks ($\times$ and $+$) for modes 1 and 2, respectively. Reconvolved picks are shown on panel (a), where some picks have been removed due to insufficient signal level.

coordinates of the recorder (considered known), $v_m(\mathbf{e},f)$ is the mode group speed which depends on the environmental model $\mathbf{e}$, and Δ_a is the recorder clock drift relative to a reference recorder. The inversion uses a trans-D Bayesian formulation which is briefly described here (see Warner *et al.*[21] for details). The range-independent environmental model $\mathbf{e}$ consists of a water column with unknown depth and SSP over a seabed consisting of an unknown number of homogeneous layers (each layer characterized by unknown thickness, sound speed, and density) overlying a half-space of unknown geoacoustic parameters. Mode group speeds are calculated for an environmental model using the normal-mode code ORCA (Ref. 23) and are converted to predicted modal arrival times using the whale source IF, location, and relative recorder clock drift [Eq. (1)], all of which are unknown model parameters to be estimated in the inversion (the model also includes error standard deviations, see Sec. II C). In a Bayesian formulation the solution consists of properties of the posterior probability density (PPD) of the model parameters given the measured data and prior information. A reversible-jump Markov-chain Monte Carlo[24] algorithm is applied to sample the PPD over a trans-D model space in which the number of SSP nodes and seabed layers can change by probabilistically accepting transitions between model parameters/parameterizations according to the Metropolis-Hastings-Green criterion.[24] The transition acceptance probability depends on the prior, proposal, and likelihood ratios, with the likelihood defined by the assumption of Gaussian-distributed errors with unknown standard deviation for each whale call (discussed below in Sec. II C). Uniform bounded priors are used for all model parameters, with an additional joint prior that constrains sub-bottom sound speed and density to physically realistic combinations.[25,26] The Markov chain samples over the number and parameters of SSP nodes and sub-bottom layers to estimate the trans-D PPD. Parallel tempering[27–30] is applied to increase the dimension-jump acceptance rate. Fixed-dimensional parameters (i.e., source IF, whale location, and relative clock drift) were found to be highly correlated and perturbations to these parameters had to be applied in principal-component (rotated) space to achieve convergence.[31]

C. Likelihood

The likelihood function is defined by the residual error distribution. These errors result from measurement, data-processing, and theory errors, the statistics of which are often unknown. The data residuals for model $\mathbf{m}_k$ are given by $\mathbf{d}-\mathbf{d}(\mathbf{m}_k)$, where $\mathbf{d}$ and $\mathbf{d}(\mathbf{m}_k)$ are the measured and predicted data (i.e., mode arrival times in seconds), respectively, and k indexes possible model parameterizations (number of SSP nodes and sub-bottom layers). In this paper, the residual errors are assumed Gaussian distributed; the validity of this assumption is checked *a posteriori*. For N data with Gaussian-distributed errors, the likelihood function is

$$L(k,\mathbf{m}_k)=\frac{1}{(2\pi)^{N/2}|\mathbf{C}_d|^{1/2}}\times\exp\left[-\frac{1}{2}\left(\mathbf{d}-\mathbf{d}(\mathbf{m}_k)\right)^T\mathbf{C}_d^{-1}\left(\mathbf{d}-\mathbf{d}(\mathbf{m}_k)\right)\right], \tag{2}$$

where $\mathbf{C}_d$ is a diagonal data covariance matrix. Some previous modal-dispersion inversions have assumed different error standard deviations between modes[21,32] but this requires many data (arrival times) for each mode to constrain each standard deviation. The whale calls analyzed for this paper have relatively few modes and frequencies per mode so this error parameterization is too granular and not appropriate here. We therefore assume error standard deviations (σ_w) that vary only between whale calls so σ_w is constant over recorder, mode, and frequency. Let $\mathbf{d}_{wam}$ represent a vector of modal arrival times at N_{wam} frequencies. The likelihood function for uncorrelated noise is the product

$$L(k,\mathbf{m}_k)=\prod_{w=1}^{W}\prod_{a=1}^{A}\prod_{m=1}^{M_{wa}}\frac{1}{\left(2\pi\sigma_w^2\right)^{N_{wam}/2}}\times\exp\left[-\frac{|\mathbf{d}_{wam}-\mathbf{d}_{wam}(\mathbf{m}_k)|^2}{2\sigma_w^2}\right],\tag{3}$$

where W is the total number of whale calls considered, A is the total number of recorders that detected at least one call, and M_{wa} is the number of modes considered for call w on recorder a. For recorders a that do not detect a particular whale call w the term within the products is replaced by unity. Substituting Eq. (1) into this equation and setting $\partial L/\partial\Delta_a=0$ leads to a maximum-likelihood estimate for the inter-recorder clock drift Δ_a

$$\hat{\Delta}_a(\mathbf{m}_k)=\frac{\sum_{w}^{W}\sum_{m}^{M_{wa}}\sum_{f}^{N_{wam}}\left[d_{wam}(f)-\tau_w(f)-|\mathbf{r}_{wa}|/v_m(f)\right]/\sigma_w^2}{\sum_{w}^{W}\sum_{m}^{M_{wa}}N_{wam}/\sigma_w^2},\tag{4}$$

where $\mathbf{r}_{wa}$ is (X_a-x_w,Y_a-y_w). Equation (4) provides an expression for Δ_a in terms of the data and the other unknown parameters which can be used to sample implicitly over Δ_a by sampling explicitly over the other parameters.[33] This formulation assumes the relative recorder clock drift does not significantly change between the first and last inverted whale calls.

III. SIMULATION STUDY

This section illustrates and verifies the inversion methodology in a simulation study based on recordings of bowhead whale calls from the Chukchi Sea (described in Sec. IV). This study considers calls from five whales at different locations about a cluster of seven asynchronous recorders, labeled A–G. The recorder locations for the simulation are taken from coordinates of a deployed recorder cluster.[22] The source IF are linear frequency up- or down-sweeps and the relative clock drifts are constant between calls. The environmental model for the simulation has two sub-bottom layers (one interface) and two water-column SSP nodes (in addition to unknown water sound speeds at the surface and bottom). The true parameter values and the bounds of the uniform prior distributions assumed for all environmental parameters are listed in Table I (Quijano *et al.*[26] describes the joint prior distribution for sub-bottom sound speed and density used here). The easting and northing prior bounds on the whale locations are ±10 km from recorder A, the source IF prior bounds are 10 s prior to the call arrival time on the reference recorder (recorder A for all calls except call 3 which had reference recorder D), and the error standard deviation prior for each whale call is uniform from 1 to 100 ms. Mode arrival times at 7 frequencies for modes 1 and 2 were simulated using Eq. (1) for each call with exact modal group speeds calculated by the normal-mode code ORCA (Ref. 23). Data were simulated for a minimum of two and up to all seven recorders, depending on the call. Gaussian-distributed errors were added to the synthetic data with standard deviations that were constant over recorders, modes, and frequencies but varied between whale calls from 12 to 17 ms. Table II lists the recorders that detected each call and the corresponding error statistics.

TABLE I. Environment parameter values and prior bounds for the simulations. Note that sub-bottom sound speed and density were further constrained by a joint prior bound.

Parameter	True value(s)	Prior
c_w at surface (m/s)	1450	[1435,1455]
c_w at seafloor (m/s)	1440	[1435,1455]
Water depth z_b (m)	41	[38,50]
# SSP nodes	2	[0,5]
SSP node depths (m)	[20,24]	[0,z_b]
SSP node $\boldsymbol{c}_w$ (m/s)	[1450,1440]	[1435,1455]
# sub-bottom interfaces	1	[0,6]
Interface depths (m)	[14.5]	[0,50]
Layer speed c_b (m/s)	[1630]	[1460,2500]
Basement c_b (m/s)	2384	[1460,2500]
Layer density ρ (g/cm^3)	[1.45]	[1.3,2.5]
Basement ρ (g/cm^3)	2.32	[1.3,2.5]

Inversions for nine scenarios were performed on the synthetic data. Scenarios 1–5 invert individual calls 1–5, respectively; scenario 6 jointly inverts all 5 calls (environmental parameters are inverted for in each scenario). Scenarios 7–9 are variations on scenario 1 that investigate the effect on localization uncertainties of knowing the SSP and/or geoacoustic parameters: scenario 7 considers known SSP but unknown geoacoustics, scenario 8 considers known geoacoustics but unknown SSP, and scenario 9 considers known SSP and geoacoustics. Inversions were performed on the synthetic datasets with approximately 500 000 samples drawn from the PPD via the trans-D Bayesian inversion and fixed-length chain thinning[34] restricted the number of samples that were saved to 100 000. All inversions were found to produce approximately Gaussian-distributed data residuals (not shown).

Figure 2 shows the two-dimensional marginal probability distributions for whale locations in scenarios 1–9. Each call distribution is normalized by its maximum value to more clearly illustrate the distribution shapes. The true whale locations are shown as the intersection of the dashed lines (lines for scenario 6, which includes all sources, are omitted to reduce clutter) and the recorders that detected calls are shown with × symbols. Inset plots at 3 times magnification are shown in some panels to illustrate small distribution shapes. The extents of the marginal distributions

TABLE II. Simulated whale call parameters.

Call	Recorders	x_w (km)	y_w (km)	σ_w (ms)
1	A–G	3	3	14
2	A–D	7	4	14
3	D, E	8	2	17
4	A–D, F, G	−2	−1	12
5	A–D, F, G	−4	3	15

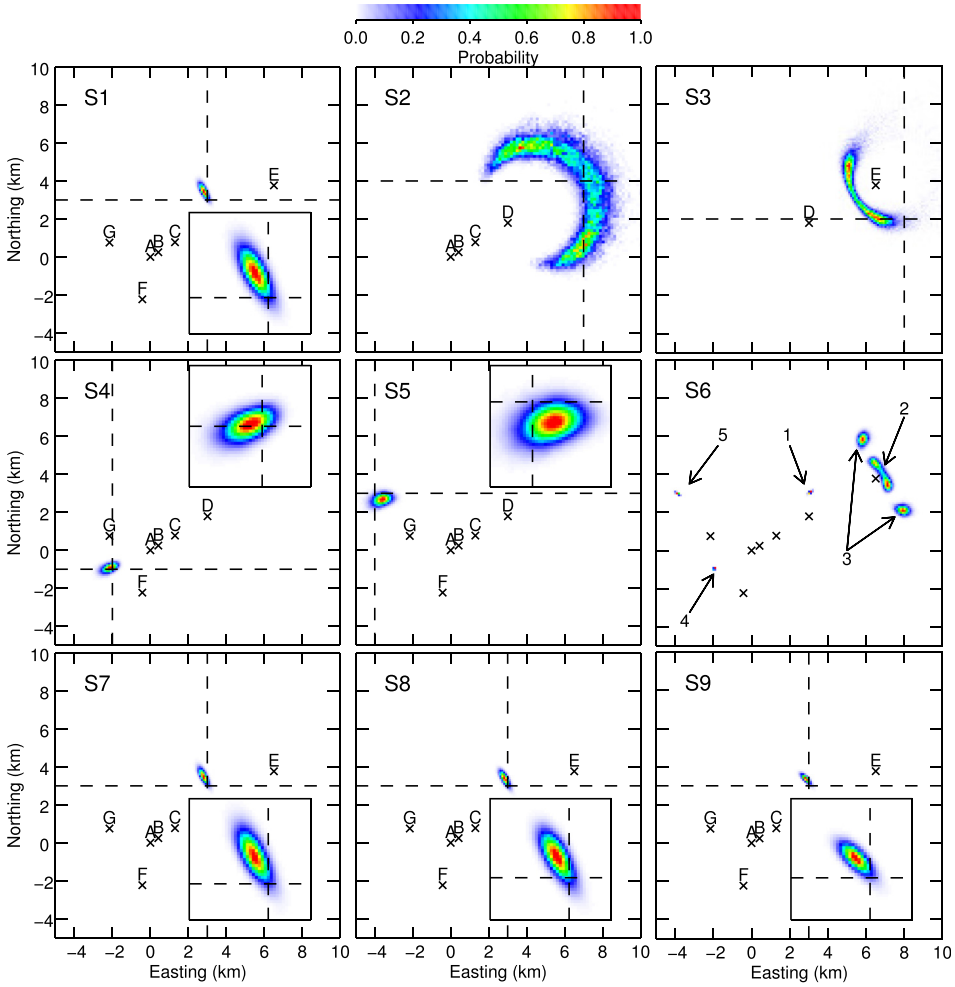

FIG. 2. (Color online) Marginal probability densities for whale location(s) in simulated scenarios 1–9 (described in text). True whale locations are shown with dashed lines (except scenario 6), and receivers that recorded the call(s) in each scenario are indicated with-× symbols. Inset plots show the corresponding distributions at 3 times magnification.

show the estimated uncertainty of the whale locations. The probability contours for scenarios 1, 4, and 5 are approximately elliptical. Scenarios 2 and 3 have relatively high uncertainties because the simulated calls were not detected on recorders off the cluster's main axis (approximately NE–SW), resulting in symmetric but non-elliptical probability contours. The localization results for scenario 6 (i.e., calls from scenarios 1–5 inverted collectively) show substantial improvement over all corresponding individual whale call inversions. The uncertainty distributions for calls 1, 4, and 5 are much narrower than those of their corresponding single-call inversions. The symmetric distribution for call 3 is well constrained but the distribution is multi-modal about the axis of the receivers D and E on which it was recorded (see scenario 3 result). Parallel tempering was found to be essential for sampling these multimodal distributions and achieving PPD convergence. Scenario 6 clearly shows the localization improvements from joint inversion of multiple whale calls. Resolution of other parameters (especially relative recorder clock drift) is also greatly improved by joint inversion and is discussed later in this section. The localization results for scenarios 7 and 8 are very similar to those of scenario 1, indicating that precise prior knowledge of the SSP and/or geoacoustic parameters does not significantly improve localization results, given that the environmental parameters are included in the inversion. Scenario 9 shows minor localization improvement when both SSP and geoacoustic parameters are known, but the improvement is much less than that from joint inversion over multiple whale calls. Table III quantifies the localization results with two-standard deviation (2SD) uncertainties of the easting and northing estimates for the simulated calls.

TABLE III. Localization results and mean residual error standard deviations ($\bar{\sigma}_w$) for inverted simulated calls. Mean location and 2SD are given as easting and northing pairs. Note that the marginal probability distribution contours for whale locations for calls 2 and 3 are not elliptical so results for these calls should be considered in the context of the marginal location probability distributions (see Fig. 2).

Call	Scenario	Mean location (km)	2SD (km)	$\bar{\sigma}_w$ (ms)
1	1	2.77,3.40	0.32,0.53	11.2
1	6	3.01,3.01	0.13,0.11	11.7
1	7	2.75,3.44	0.32,0.54	11.6
1	8	2.78,3.32	0.32,0.51	11.8
1	9	2.79,3.29	0.30,0.32	11.9
2	2	5.98,3.61	3.34,4.40	15.3
2	6	6.76,3.95	0.65,1.03	15.6
3	3	5.92,3.46	2.01,2.93	18.7
3	6	6.83,3.94	2.13,3.72	19.5
4	4	−2.23,−0.98	0.53,0.34	12.4
4	6	−2.00,−0.99	0.02,0.02	12.4
5	5	−3.70,2.64	0.67,0.44	14.0
5	6	−3.92,2.94	0.13,0.08	14.6

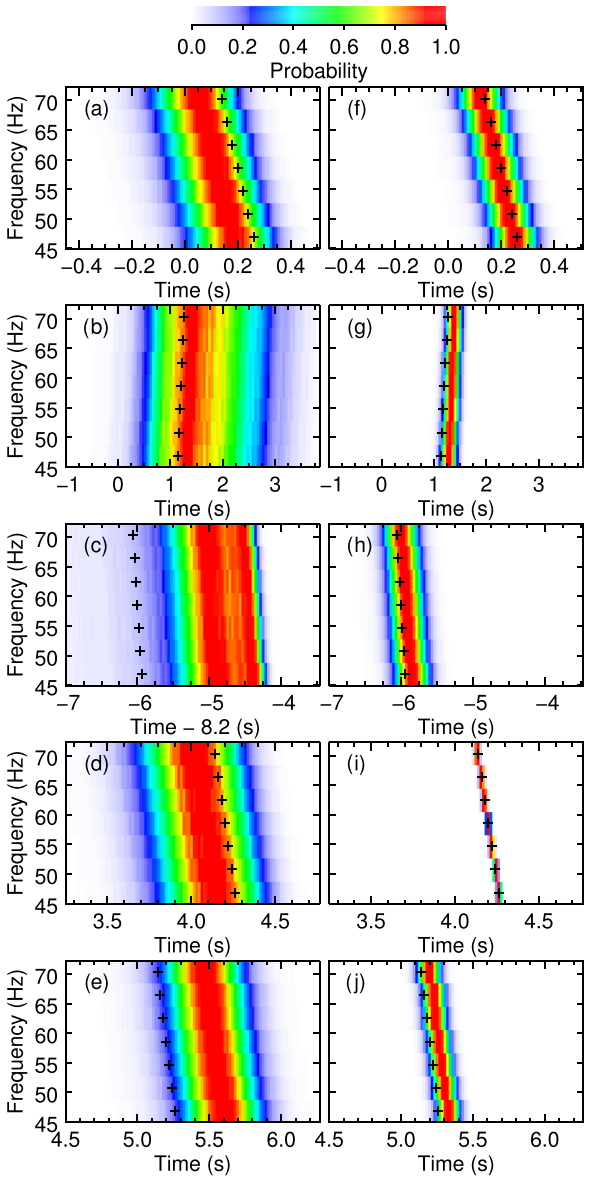

FIG. 3. (Color online) Normalized marginal probability densities for simulated whale call source IF in scenarios 1–5 [panels (a)–(e)] and scenario 6 [(f)–(j)]. True source IF are shown with + symbols.

Figure 3 shows the normalized marginal distributions for source IF 1–5 in scenarios 1–6. The left panels show source IF for calls in scenarios 1–5 (inverted individually) and the right panels show the source IF for the same calls in scenario 6 (inverted jointly). Note that scenario 3 [panel (c)] had reference recorder D (since only recorders D and E detected the call). To compare source IF distributions for this scenario with scenario 6, which had reference recorder A, estimated and true times for scenario 3 were adjusted to account for the difference in reference recorders using the true relative clock drift (−8.2 s). In all scenarios the shape of the source IF is well resolved and most of the mismatch is associated with a frequency-independent time shift that is due to uncertainties of the relative recorder clock drifts and/or source locations. The time shifts are more accurately constrained in scenario 6 due to the smaller uncertainty on source locations and clock drifts (the latter is discussed later in this section).

Figure 4 shows the marginal probability profiles for the SSP and geoacoustic parameters for scenarios 1 and 6 (corresponding results for scenarios 2–5 are similar to those of scenario 1 and are omitted for brevity). These profiles are normalized independently at each depth to more clearly illustrate the range of values, and the corresponding probability ratio profiles to the right of the marginal profiles indicate the relative scaling. This figure also shows the marginal profiles for the SSP-node and sub-bottom-interface depths.

The marginal SSP distribution is relatively uniform over depth in scenario 1, indicating that little structure is resolved by the data. The node depth distribution is uniform over most of the water column but decreases to zero near the bottom (over the prior bounds for water depth). The marginal distributions for the number of SSP nodes and for the water depth are approximately uniform (not shown). Higher-order modes, which have smaller mode function wavelengths (in depth), are required for resolving finer-scale SSP structure.[21] The geoacoustic probability profiles agree well with the true profile given their uncertainties. Sub-bottom sound speed and density are resolved within their prior bounds; however, the resolution for density within the prior bounds is primarily due to the joint-prior bound with sound speed.

The corresponding results for scenario 6 show some narrowing of the SSP probability distribution in the lower portion of the water column but the overall shape of the SSP is not resolved. The geoacoustic profiles are similar to those of scenario 1. This suggests there is little benefit to inverting multiple whale calls in terms of environmental resolution; however, there could be more benefit if multiple whale calls cover different frequency ranges and/or more modes are present.

Table IV lists the mean recorder clock drifts relative to reference recorder A and the estimated (two-standard deviation) uncertainties. The single call inversions (scenarios 1–5 and 7–9) provide estimated clock drifts with uncertainties that vary between 8 and 739 ms. Drift uncertainties are correlated with distance from the reference recorder (e.g., drift uncertainties for B, the closest recorder to A, were typically lowest) and anticorrelated with the number of recorders that detected the call. Each detection provides a source-receiver range estimate, and having more range estimates better constrains the whale location, which in turn improves clock drift estimates. The multi-call inversion (scenario 6) produced significantly reduced drift uncertainties compared to the single call inversions. Each whale call constrains the drifts in different ways and to different degrees. The multi-call inversion requires that all data are fit simultaneously, which requires an effective averaging of the drift estimates. The benefit comes from having multiple whale calls at locations spread out among the hydrophone cluster (inverting multiple calls from a single location would not improve drift estimates to this extent). The drift uncertainty reduction from a multi-call localization approach increases with the number of calls detected on a given recorder provided the magnitude of the drift uncertainties for individual-call inversions is relatively consistent. For example, the uncertainty for Δ_C decreases by a factor of 3.5 (relative to the smallest

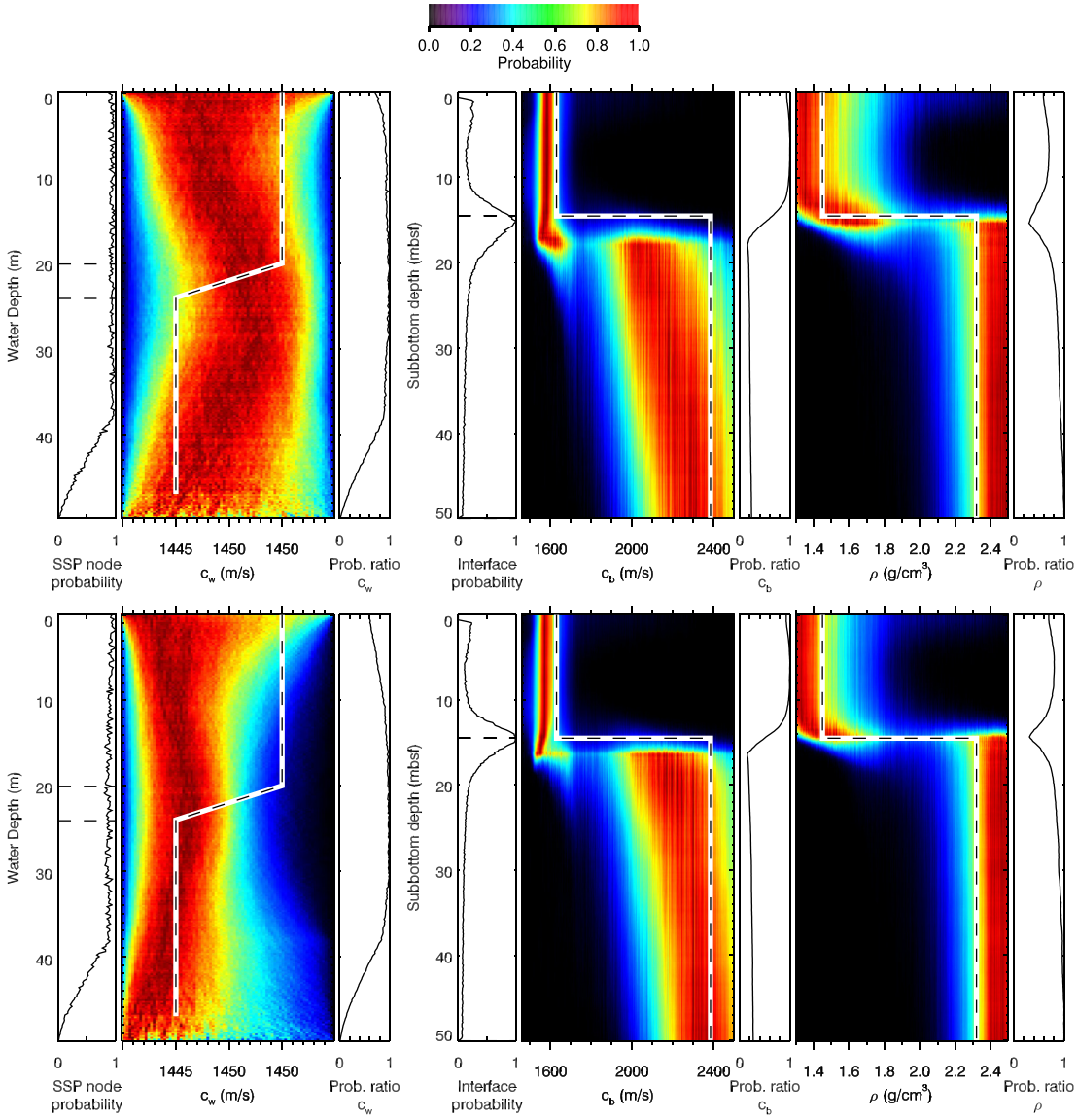

FIG. 4. (Color online) Marginal probability profiles for water SSP and bottom sound speed and density, together with their corresponding node/interface depth profiles and depth normalization profiles. Top and bottom panels show results from simulation scenarios 1 (single whale call) and 6 (multiple whale calls). Plot bounds are the prior bounds for SSP and geoacoustic parameters, although sub-bottom sound speed and density are further constrained by a joint prior distribution. True parameter values are shown with dashed lines.

TABLE IV. True and estimated mean relative recorder clock drifts (relative to recorder A) and two standard deviation uncertainties (s) for the simulation scenarios. Note that estimated clock drift for scenario 3 has been adjusted to account for the difference in reference recorders (D vs A in scenarios 3 and 6, respectively) using the true relative clock drift (−8.2 s) to allow direct comparison with results in other scenarios.

Scenario	Δ_B	Δ_C	Δ_D	Δ_E	Δ_F	Δ_G
True	14.1	18.3	8.2	−2.3	−20.8	−3.4
1	14.09,0.018	18.25,0.065		−2.32,0.252	−20.85,0.063	−3.27,0.162
2	14.08,0.042	18.22,0.157	7.88,0.569			
3				−2.88,0.739		
4	14.11,0.008	18.31,0.014	8.22,0.025		−20.80,0.253	−3.25,0.283
5	14.10,0.039	18.28,0.105	8.14,0.184		−20.78,0.166	−3.39,0.117
6	14.10,0.004	18.30,0.004	8.20,0.010	−2.27,0.227	−20.80,0.014	−3.40,0.009
7	14.09,0.018	18.24,0.067		−2.31,0.258	−20.86,0.063	−3.26,0.165
8	14.09,0.017	18.25,0.063		−2.35,0.252	−20.84,0.066	−3.29,0.159
9	14.09,0.014	18.26,0.049		−2.36,0.227	−20.85,0.054	−3.30,0.117

uncertainty from the single-call inversions) but the uncertainty for Δ_E, which is only estimated in scenarios 1 and 3, only decreases by a factor of 1.1; data in scenario 3 do not add much information because uncertainty is significantly higher than that in scenario 1. The clock drift uncertainties for scenarios 7–9 show some improvement compared to scenario 1, but the improvement is much less than that from joint inversion. This indicates that prior environmental knowledge does not significantly improve clock drift estimates, provided the baseline inversion treats the environment as unknown.

Figure 5 shows the fit to the data achieved in scenario 1 including the synthetic (noisy) arrival times, 5th and 95th percentiles for predicted arrival times calculated from a random sample of 5000 models from the PPD, and the (error-free) theoretical arrival times calculated from Eq. (1). The inversion sampled models that produce predicted times in good agreement with the synthetic noisy arrival time data. Fits to the data for other scenarios were similar and are not shown here for brevity; however, the mean standard deviations for residuals in all simulated scenarios are summarized in Table III and were within 2.8 ms of the true values in Table II.

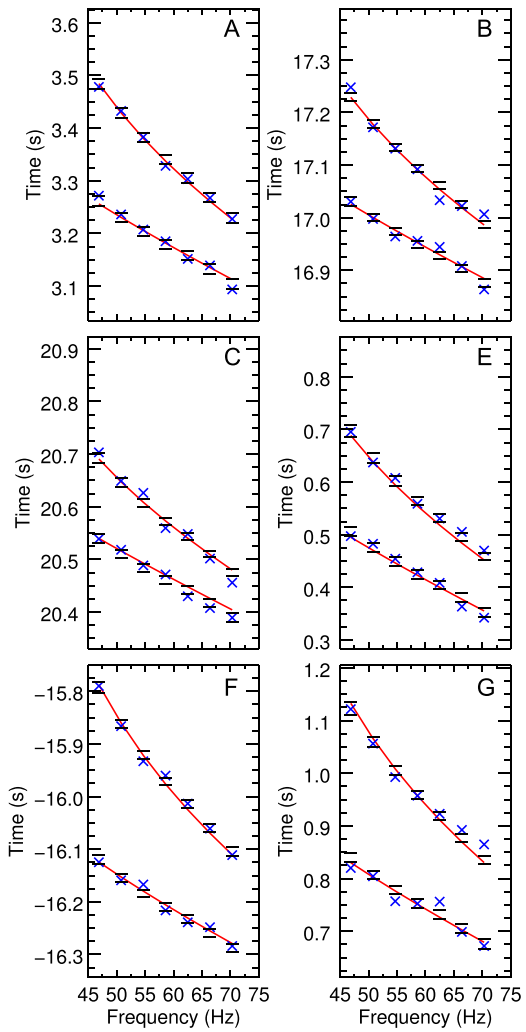

FIG. 5. (Color online) Mode arrival times for simulated whale call 1 on recorders A–C, E–G (the call was not detected on recorder D in scenario 1). True (error-free) arrival times (solid curves), noisy synthetic data (×), and the 5th and 95th percentile predicted arrival times calculated from a random sample of models from the PPD (solid horizontal lines) are shown for each recorder.

IV. BOWHEAD WHALE CALL DATA

Long-term underwater acoustic recordings were collected by JASCO Applied Sciences from August to October 2013 as part of an acoustic measurement program designed, in part, to record marine mammal calls over a large area of the Chukchi Sea.[22] The recordings were made using 28 of JASCO's Autonomous Multichannel Acoustic Recorders (AMARs) (JASCO Applied Sciences, Dartmouth, Nova Scotia, Canada), each equipped with a single Geospectrum M8E hydrophone (GeoSpectrum Technologies Inc, Dartmouth, Nova Scotia, Canada) (nominal sensitivity −164 dB re 1 V/μPa). Most of the recorders were spaced tens of kilometers apart; however, a cluster of closely-spaced recorders was centered around Shell's 2012 drilling location to quantify sound levels from oil and gas exploration activities. Seven recorders (denoted by JASCO as BGA–BGE, BGH, and BGJ, but herein renamed as A–G, respectively) were deployed within 8 km of the drill site (71°18.5′N, 163°12.7′W) at nominal distances of 0.5, 1, 2, 4, and 8 km (three AMARs were deployed at 2-km range at different azimuths) and recorded 24-bit samples at 64 kHz. The water depths at the 7 AMAR locations ranged between 46.0 and 48.7 m, so based on this relatively flat bathymetry, the environment is approximated as range-independent with an unknown (effective) water depth.

Bowhead whales passed the AMAR cluster during their annual fall migration from the Beaufort and Chukchi Seas to the Bering Sea. The AMARs recorded thousands of bowhead calls and many of the calls were detected on multiple AMARs in the cluster. Some of these calls were at low frequencies (35–97 Hz) and contained significant energy in at least two dispersive modes. For this study, mode arrival times for nine bowhead calls recorded on up to all seven AMARs (A–G) were estimated as described in Sec. II A. The same call was identified by listening to the recordings and observing similar TF characteristics of the call. The calls spanned a 3.25 min period on October 11; we do not expect the relative AMAR clock drifts to change significantly over this short period. Table V lists the recorders, frequency ranges, and number of mode arrival times (N) for each call. Figure 6 shows spectrograms of the nine calls and Fig. 7

TABLE V. Inverted Bowhead whale call parameters.

Call	AMARs	Frequency range (Hz)	N
1	A–G	47–81	129
2	A–D, F, G	35–85	101
3	A, B, D–G	54–70	41
4	A–G	43–70	90
5	A, B, D–G	54–66	39
6	A–G	50–66	53
7	A, B, D–G	54–66	45
8	A–G	50–66	56
9	A–C, E–G	74–97	54

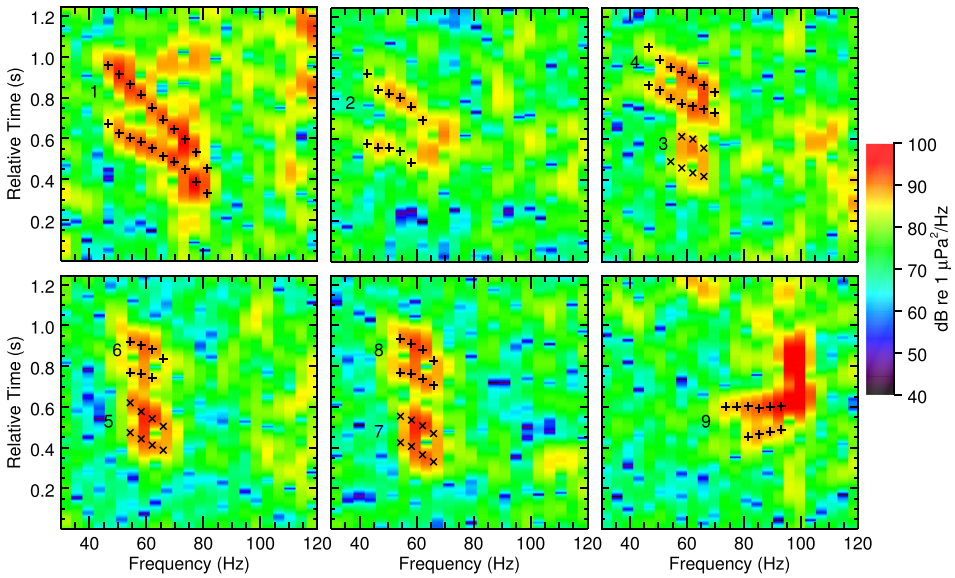

FIG. 6. (Color online) Spectrograms of whale calls recorded on AMAR A for all calls considered. Call numbers are vertically centered to the left of modes 1 and 2 of each call. Data picks (see method described in Sec. II A and illustrated in Fig. 1) are shown with + and × symbols. Note that calls 3–8 are received within an ∼8 s period.

shows spectrograms for call 1 for recordings on all seven AMARs. The relative modal dispersion that is clearly visible in Fig. 7 indicates that the whale was closest to AMAR D or E (since these recordings show the least dispersion).

Whale call inversions used the same environmental prior bounds as in the simulation study (see Table I), except the effective water depth bounds were expanded to [35, 55] m and water sound speed bounds were [1439, 1465] m/s based on historical SSP measurements in the area.[35] Location, source IF, and error standard deviation prior bounds were the same as in the simulation study.

V. INVERSION RESULTS

The trans-D Bayesian inversion was applied to each of the nine whale calls independently (scenarios 1–9) and then jointly for one multi-call inversion (scenario 10). The inversions were carried out on a parallel computer cluster with each inversion using 32 (2.1 GHz) central processing unit cores. The independent inversions took approximately 24 h to reach convergence and the joint inversion, with many more parameters to estimate, took approximately 72 h. Figure 8 shows the two-dimensional marginal probability distributions for whale locations for all scenarios, with the recorders that detected calls shown with × symbols. Each call distribution is normalized by its maximum value to more clearly illustrate the distribution shapes. Inset plots at 3 times magnification are shown in some panels to illustrate small distribution shapes. Most probability contours are approximately elliptical; however, the distribution in scenario 9 is curved and wider than the others. The distributions for calls 3–8 overlap

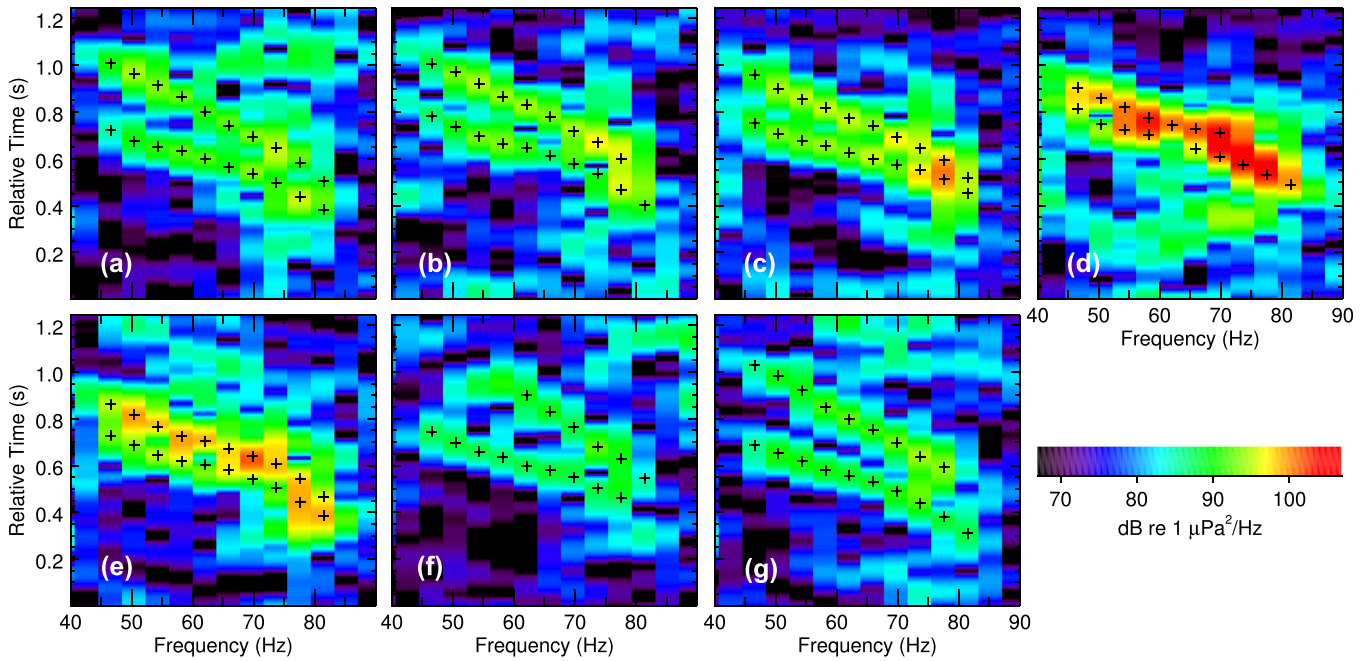

FIG. 7. (Color online) Spectrograms of whale call 1 recorded on each AMAR. Data picks are shown with + symbols.

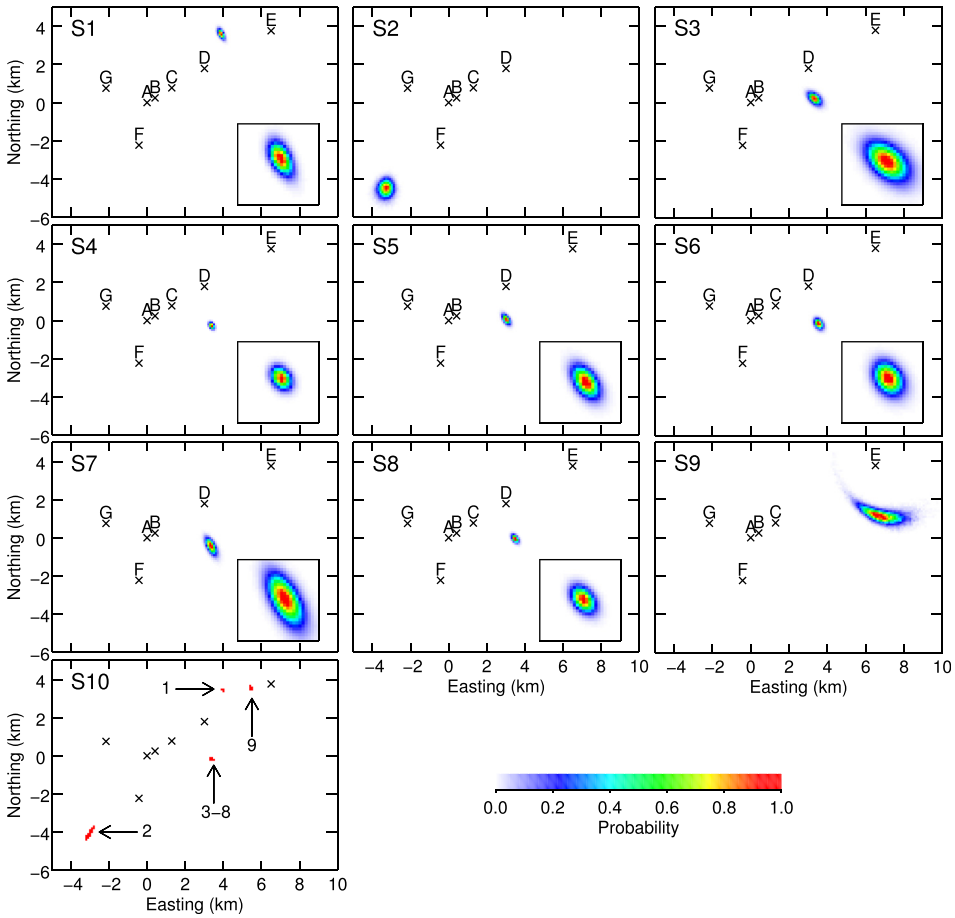

FIG. 8. (Color online) Marginal probability densities for bowhead whale location(s) for scenarios 1–10 (described in text). Probability distributions for scenario 10 are compact and are shown as a binary image for clarity. Receivers that recorded the call(s) in each scenario are indicated with × symbols. Inset plots show the corresponding distributions at 3 times magnification.

substantially, so it is not possible to conclude if the calls are coming from a single whale or multiple whales. The distributions for the multi-call inversion are substantially narrower than their corresponding single-call inversion distributions, similar to findings in the simulation study. The most-probable locations for calls 1–8 are consistent (within uncertainties) between the single- and multi-call inversions, but the location for call 9 moves a few kilometers from the peak of the single-call inversion distribution; this is discussed below with respect to the relative recorder clock drifts. Table VI lists the localization results and uncertainties for all bowhead whale calls considered.

TABLE VI. Localization results and mean residual error standard deviations ($\bar{\sigma}_w$) for inverted bowhead calls. Mean location and 2SD are given as easting and northing pairs.

Call	Scenario	Mean Location (km)	2SD (km)	$\bar{\sigma}_w$ (ms)
1	1	3.83,3.58	0.21,0.33	10.9
1	10	3.93,3.42	0.03,0.02	12.0
2	2	−3.38,−4.57	0.52,0.63	12.7
2	10	−3.07,−4.12	0.08,0.14	16.8
3	3	3.28,0.15	0.42,0.41	10.5
3	10	3.32,−0.21	0.03,0.02	10.0
4	4	3.33,−0.33	0.17,0.21	9.5
4	10	3.33,−0.21	0.03,0.02	11.4
5	5	2.97,0.01	0.25,0.33	9.7
5	10	3.33,−0.22	0.03,0.02	9.7
6	6	3.49,−0.24	0.28,0.33	10.9
6	10	3.33,−0.23	0.03,0.02	16.2
7	7	3.31,−0.50	0.36,0.55	11.7
7	10	3.31,−0.22	0.03,0.02	11.6
8	8	3.43,−0.08	0.22,0.26	8.3
8	10	3.33,−0.21	0.03,0.03	19.6
9	9	6.80,1.16	1.56,0.77	7.0
9	10	5.38,3.53	0.03,0.04	11.2

Figure 9 shows the normalized marginal distributions for the source IF. The left panels show source IF for the individual-call inversions and the right panels show the corresponding source IF for the joint inversion. The shapes of the source IF are well resolved for all calls and most of the mismatch is attributed to uncertainty in whale location and relative recorder clock drift which produces strongly correlated source IF over frequency. The distributions are much more tightly constrained in the joint inversion due to the smaller uncertainty of whale location and relative clock drift (the latter is discussed later in this section).

Figure 10 shows the marginal probability profiles for the SSP and geoacoustic parameters for scenarios 1 and 10. The corresponding results for single-call inversions 2–9 (not shown) are similar to those of scenario 1 but vary somewhat in the upper sediment layer thickness and sound speed (although the profiles are consistent within their estimated uncertainties).

In scenario 1, little SSP structure is resolved by the data and the distribution of the number of SSP nodes is uniform (not shown). The limited SSP resolution, particularly with depth, is likely due to the large wavelengths of the low-order mode functions. The node depth distribution is uniform over

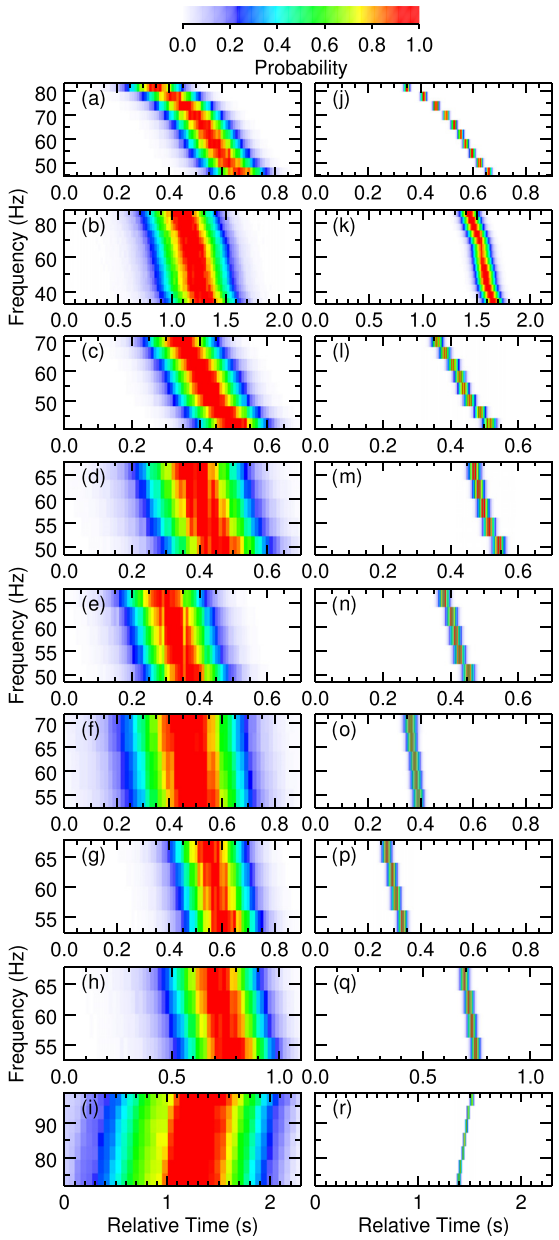

FIG. 9. (Color online) Normalized probability densities of source IF for calls 1–9 inverted independently [(a)–(i)] and jointly [(j)–(r)].

the water column but decreases to zero over the prior bounds for effective water depth. The marginal distribution for the number of sub-bottom interfaces (not shown) is peaked at zero and decreases for increasing numbers of interfaces; little sub-bottom structure is resolved by the single-call data. Sub-bottom sound speed and density are resolved within their prior bounds; however, the resolution for density is only due to the joint-prior bound with sound speed.

The corresponding results for the multi-call inversion show some SSP structure, though the upper and lower portions of the profile are very uncertain. The sound speed at mid-depth in the water column is approximately 1450 m/s which is reasonable for this Arctic region in the fall.[36] The geoacoustic profiles are similar to those of call 1 but the prominent interface depth is constrained between approximately 15 and 28 m below the seafloor (mbsf), below which the parameters are very uncertain. Figure 11 compares the top 5 mbsf sub-bottom sound speed distribution from scenario 10 to that from a recent geoacoustic inversion based on dispersion of airgun signals (with 5 modes) at a site ~16 km away from AMAR A.[21] The distributions peak at different bottom sound speeds but the distribution from the bowhead whale call inversion has heavy tails that overlap with the higher-resolution distribution from the airgun modal dispersion inversion.

Figure 11 also shows the marginal distributions for effective water depth and the shaded region indicates the range of water depths measured during AMAR deployments. The distributions for scenarios 1–9 overlap with the water depth measurements but vary in width and most-probable depth. The distribution for scenario 10 is more constrained than the ensemble of distributions from single-call inversions and has standard deviation of 1.7 m.

Table VII lists the mean relative AMAR clock drifts (to reference AMAR A) and the estimated uncertainties. The single call inversions provide estimated clock drifts with uncertainties that varied between 8 and 728 ms. Drift uncertainties are correlated with distance from the reference recorder and strongly reflect localization uncertainty (e.g., drift uncertainties on AMARs F and G for call 9 are relatively large which is reflective of the large position uncertainty perpendicular to the main axis of the AMAR cluster). The multi-call inversion (scenario 10) produced significantly reduced drift uncertainties compared to the corresponding single call inversions with estimated uncertainties of 3 to 26 ms (a reduction of up to 96%).

The fit to the data achieved in scenario 1 is shown in Fig. 12 including the picked arrival times and the 5th and 95th percentiles for estimated arrival times, calculated from a random sample of 5000 models from the PPD. The inversion sampled models that produce predicted times in excellent agreement with the picked times. Fits to the data for other scenarios were similar and are not shown here for brevity; however, the standard deviations for the residuals in all scenarios are quantified in Table VI. The call standard deviations generally increased somewhat for the multi-call scenario because all calls had to be fit with a single environmental model and set of relative clock drift parameters.

VI. SUMMARY AND CONCLUSION

This paper presented Bayesian inversion of low-frequency bowhead whale call modal dispersion data (both simulated and measured) received at a cluster of asynchronous hydrophones. Mode arrival times were determined from TF analysis of calls after filtering individual modes using a modified warping procedure that accounted for a non-impulsive source. The arrival times were then used in the inversion to estimate the whale location, source IF, water sound-speed profile, sub-bottom geoacoustic properties, and relative recorder clock drifts, all with estimated uncertainties. A trans-D framework was applied for the water-column SSP and sub-bottom geoacoustic layering properties to account for uncertainty in model parameterization.

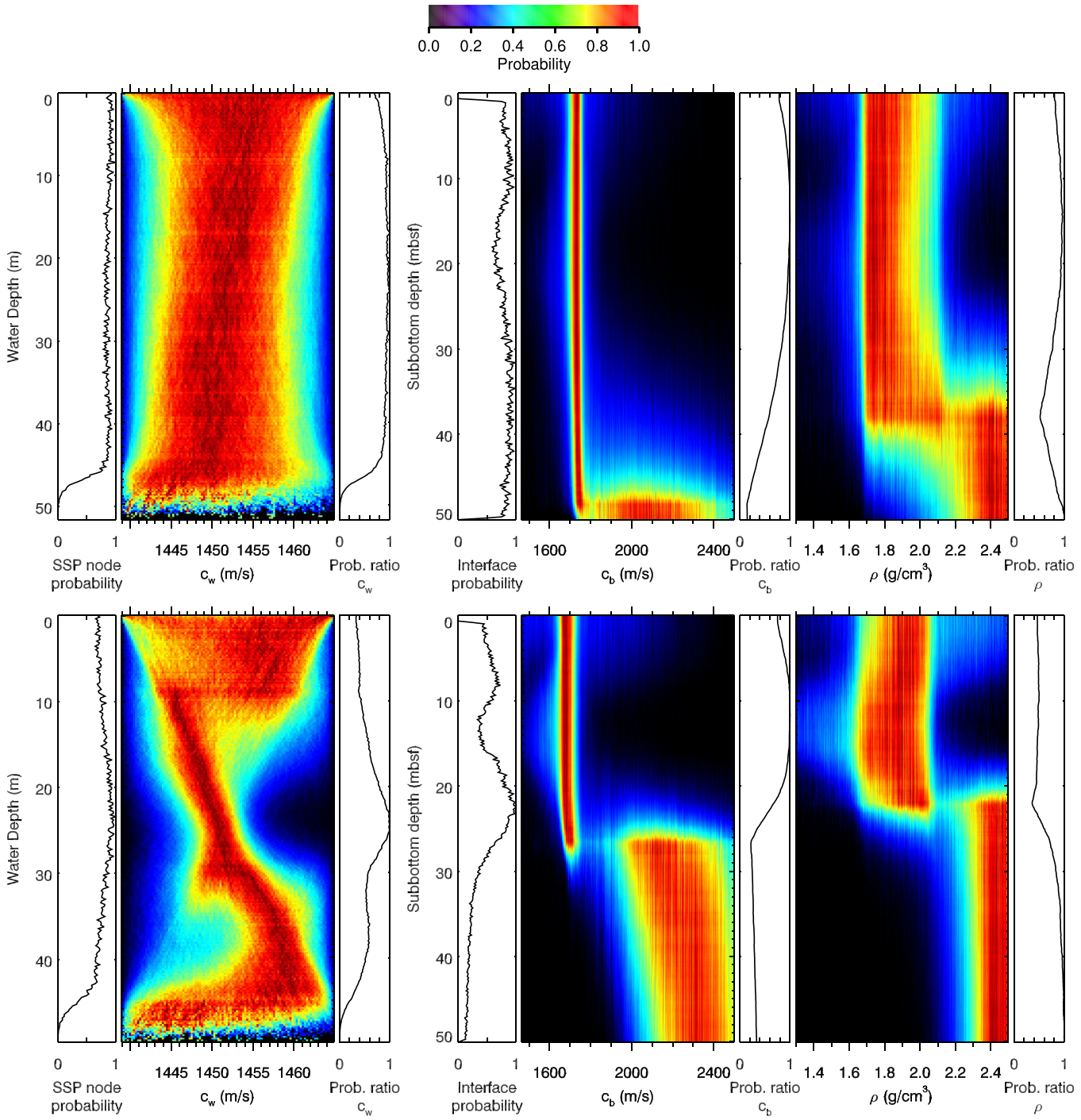

FIG. 10. (Color online) Marginal probability profiles for water SSP and bottom sound speed and density, together with their corresponding node/interface depth profiles and depth normalization profiles. Top and bottom panels show results from scenarios 1 (call 1) and 10 (calls 1–9). Plot bounds are the prior bounds for SSP and geoacoustic parameters, though sub-bottom sound speed and density are further constrained by a joint prior distribution.

A simulation study characterized the ability of the inversion to estimate the unknown parameters. Joint inversion of multiple calls was found to substantially decrease whale location and recorder clock drift uncertainties compared to single-call inversions. Exact prior knowledge of the SSP and/or geoacoustic properties was found to produce a relatively small improvement in localization and clock drift uncertainties. The inverted data provided little information on the SSP and water depth which may be due to the low frequencies and low-order modes (1 and 2) used for the simulation. The estimates of the geoacoustic profiles, whale call source IF, and relative recorder clock drifts were consistent with the true values within the estimated uncertainties.

Inversion results for bowhead whale calls recorded in the Chukchi Sea showed similar effects to the simulation study. The localization and relative recorder clock drift results improved substantially when including multiple calls in the same inversion. The SSP and sub-bottom density were not resolved but the estimated effective water depth was

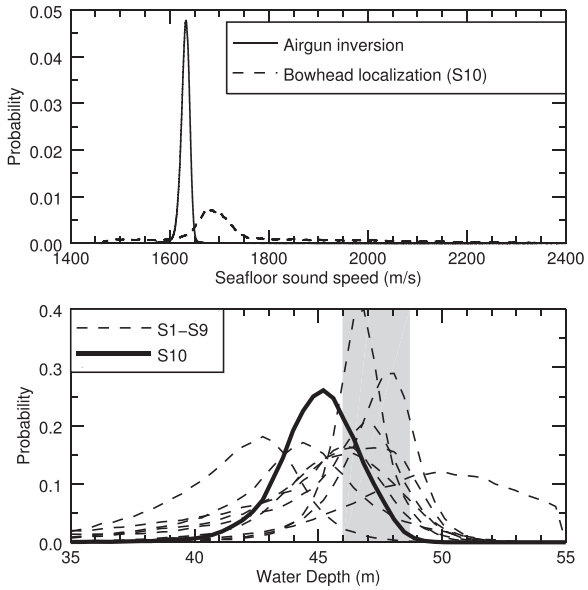

FIG. 11. Top: Marginal distributions for sub-bottom sound speed in the top 5 mbsf from inversion of airgun modal dispersion (Ref. 21) and bowhead whale call data (scenario 10). Bottom: Marginal distribution for effective water depth from separate (S1–S9) and joint (S10) inversions, with the water depths measured during AMAR deployments indicated by the shaded region.

constrained in the multi-call inversion and agreed with water depth measurements. The resolution of seabed sound speed was much less than that found in a previous Chukchi Sea study of modal dispersion inversion of airgun data which exploited the impulsive nature of the source and involved a higher modal content (up to five modes compared to only two in the whale-call data).

Overall, modal dispersion data and the trans-D inversion approach are shown to be capable of estimating locations of bowhead whales several kilometers from an asynchronous hydrophone cluster to accuracies of 30–160 m in an uncertain range-independent environment. This localization accuracy is sufficient for determining if marine mammals are exposed to sound levels above specific thresholds (so that mitigation strategies can be implemented). The inversion also resolved relative recorder clock drift to uncertainties less than 30 ms. This synchronization is sufficient for localizing marine mammals using other types of calls that are not suitable for mode arrival time estimation (e.g., using time-difference-of-arrival data). Whale

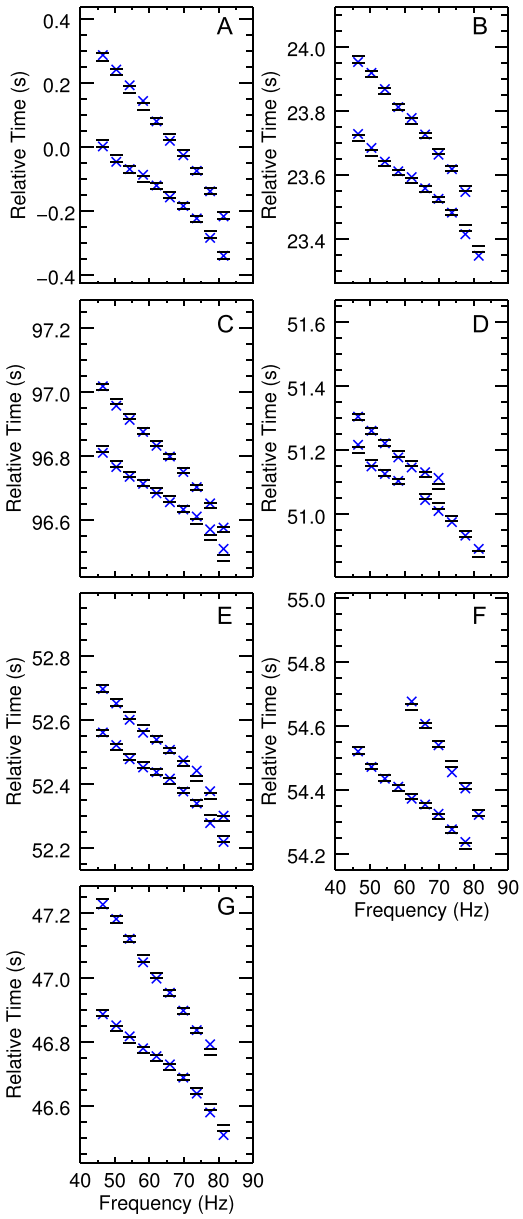

FIG. 12. (Color online) Mode arrival times for whale call 1 (× symbols) on recorders A–G, and the 5th and 95th percentile predicted arrival times calculated from a random sample of models from the PPD (horizontal lines).

TABLE VII. Estimated relative AMAR clock drifts and two standard deviation uncertainties (s) for the bowhead whale call inversions.

Scenario	Δ_B	Δ_C	Δ_D	Δ_E	Δ_F	Δ_G
1	24.04,0.008	97.84,0.022	53.49,0.090	54.34,0.214	53.13,0.046	45.91,0.079
2	24.07,0.015	97.86,0.034	53.59,0.065		53.19,0.105	45.92,0.153
3	24.04,0.028		53.75,0.284	54.50,0.432	52.99,0.177	45.88,0.047
4	24.04,0.015	97.80,0.054	53.47,0.135	54.34,0.188	53.20,0.090	45.86,0.018
5	24.05,0.024		53.47,0.203	54.09,0.254	53.03,0.149	45.88,0.034
6	24.04,0.023	97.84,0.081	53.62,0.218	54.56,0.308	53.18,0.136	45.87,0.027
7	24.04,0.038		53.33,0.259	54.22,0.313	53.27,0.240	45.84,0.029
8	24.05,0.017	97.88,0.063	53.70,0.161	54.59,0.224	53.12,0.108	45.90,0.025
9	24.02,0.016	97.75,0.054		53.60,0.728	53.62,0.203	45.54,0.101
10	24.04,0.003	97.84,0.003	53.54,0.009	54.39,0.026	53.16,0.007	45.87,0.005

tracking and marine mammal density estimation may be possible using such an approach since it can be applied to a much larger dataset of marine mammal vocalizations. Performing modal dispersion-based localization and synchronization at multiple times throughout a long-duration recording could provide information on relative recorder clock drift rates.

ACKNOWLEDGMENTS

The authors thank Julien Bonnel of ENSTA Bretange for his code to perform the mode warping, Louis Brzuzy of SEPCO for allowing us to publish results from the Chukchi Sea study, and three anonymous reviewers and associate editor Aaron Thode for reviewing and improving the manuscript. G.A.W. was supported by JASCO Applied Sciences and a NSERC Industrial Postgraduate Scholarship. The inversions were carried out on a computer cluster operated by the authors and funded by NSERC and ONR Ocean Acoustics.

[1]W. J. Richardson, B. Würsig, and C. R. Greene, "Reactions of bowhead whales, *Balaena mysticetus*, to seismic exploration in the Canadian Beaufort Sea," J. Acoust. Soc. Am. **79**, 1117–1128 (1986).
[2]S. B. Blackwell, C. S. Nations, T. L. McDonald, C. R. Greene, A. M. Thode, M. Guerra, and A. M. Macrander, "Effects of airgun sounds on bowhead whale calling rates in the Alaskan Beaufort Sea," Marine Mam. Sci. **29**, E342–E365 (2013).
[3]D. E. Hannay, J. Delarue, X. Mouy, B. S. Martin, D. Leary, J. N. Oswald, and J. Vallarta, "Marine mammal acoustic detections in the northeastern Chukchi Sea, September 2007–July 2011," Cont. Shelf Res. **67**, 127–146 (2013).
[4]L. T. Quakenbush, J. J. Citta, J. C. George, R. J. Small, and M. P. Heide-Jørgensen, "Fall and winter movements of bowhead whales (*Balaena mysticetus*) in the Chukchi Sea and within a potential petroleum development area," Arctic **63**, 289–307 (2010).
[5]S. E. Moore and R. R. Reeves, "Distribution and movement," in *The Bowhead Whale*, edited by J. J. Burns, J. J. Montague, and C. J. Cowles (Society for Marine Mammalogy, Lawrence, KS, 1993), Vol. 2, pp. 313–388.
[6]S. B. Blackwell, C. S. Nations, T. L. McDonald, A. M. Thode, D. Mathias, K. H. Kim, C. R. Greene, and A. M. Macrander, "Effects of airgun sounds on bowhead whale calling rates: Evidence for two behavioral thresholds," PloS One **10**, 1–29 (2015).
[7]C. T. Mitchell, ed., *Arctic Seismic Synthesis and Mitigating Measures Workshop Proceedings* (Minerals Management Service, Barrow, AK, 1997).
[8]C. W. Clark and J. H. Johnson, "The sounds of the bowhead whale, *Balaena mysticetus*, during the spring migrations of 1970 and 1980," Can. J. Zool. **62**, 1436–1441 (1984).
[9]C. R. Greene, M. W. McLennan, R. G. Norman, T. L. McDonald, R. S. Jakubczak, and W. J. Richardson, "Directional frequency and recording (DIFAR) sensors in seafloor recorders to locate calling bowhead whales during their fall migration," J. Acoust. Soc. Am. **116**, 799–813 (2004).
[10]A. M. Thode, K. H. Kim, S. B. Blackwell, C. R. Greene, C. S. Nations, T. L. McDonald, and A. M. Macrander, "Automated detection and localization of bowhead whale sounds in the presence of seismic airgun surveys," J. Acoust. Soc. Am. **131**, 3726–3747 (2012).
[11]S. H. Abadi, A. M. Thode, S. B. Blackwell, and D. R. Dowling, "Ranging bowhead whale calls in a shallow-water dispersive waveguide," J. Acoust. Soc. Am. **136**, 130–144 (2014).
[12]C. W. Clark and W. T. Ellison, "Calibration and comparison of the acoustic location methods used during the spring migration of the bowhead whale, *Balaena mysticetus*, off Pt. Barrow, Alaska, 1984-1993," J. Acoust. Soc. Am. **107**, 3509–3517 (2000).
[13]A. M. Thode, P. Gerstoft, W. C. Burgess, K. G. Sabra, M. Guerra, M. D. Stokes, M. Noad, and D. H. Cato, "A portable matched-field processing system using passive acoustic time synchronization," IEEE J. Ocean. Eng. **31**, 696–710 (2006).
[14]Y.-T. Lin, A. E. Newhall, and J. F. Lynch, "Low-frequency broadband sound source localization using an adaptive normal mode back-propagation approach in a shallow-water ocean," J. Acoust. Soc. Am. **131**, 1798–1813 (2012).
[15]A. E. Newhall, Y.-T. Lin, J. F. Lynch, M. F. Baumgartner, and G. G. Gawarkiewicz, "Long distance passive localization of vocalizing Sei whales using an acoustic normal mode approach," J. Acoust. Soc. Am. **131**, 1814–1825 (2012).
[16]S. M. Wiggins, M. A. McDonald, L. M. Munger, S. E. Moore, and J. A. Hildebrand, "Waveguide propagation allows range estimates for North Pacific right whales in the Bering Sea," Can. Acoust. **32**, 146–154 (2004).
[17]J. Bonnel, A. M. Thode, S. B. Blackwell, K. Kim, and A. M. Macrander, "Range estimation of bowhead whale (*Balaena mysticetus*) calls in the arctic using a single hydrophone," J. Acoust. Soc. Am. **136**, 145–155 (2014).
[18]F. B. Jensen, W. A. Kuperman, M. B. Porter, and H. Schmidt, *Computational Ocean Acoustics, Series in Modern Acoustic and Signal Processing* (AIP Press, New York, 1993), pp. 271–333.
[19]L. Cohen, *Time-Frequency Analysis* (Prentice Hall PTR, Englewood Cliffs, New Jersey, 1995), pp. 27–43.
[20]J. Bonnel, B. Nicolas, J. I. Mars, and S. C. Walker, "Estimation of modal group velocities with a single receiver for geoacoustic inversion in shallow water," J. Acoust. Soc. Am. **128**, 719–727 (2010).
[21]G. A. Warner, S. E. Dosso, J. Dettmer, and D. E. Hannay, "Bayesian environmental inversion of airgun modal dispersion using a single hydrophone in the Chukchi Sea," J. Acoust. Soc. Am. **137**, 3009–3023 (2015).
[22]J. Delarue, J. MacDonnell, B. Martin, X. Mouy, and D. Hannay, "Northeastern Chukchi Sea joint acoustic monitoring program 2012-2013," Technical Report 00808, JASCO Applied Sciences (2014).
[23]E. K. Westwood, C. T. Tindle, and N. R. Chapman, "A normal mode model for acousto-elastic ocean environments," J. Acoust. Soc. Am. **100**, 3631–3645 (1996).
[24]P. J. Green, "Reversible jump Markov chain Monte Carlo computation and Bayesian model determination," Biometrika **82**, 711–732 (1995).
[25]D. R. Jackson and M. D. Richardson, *High-Frequency Seafloor Acoustics*, 1st ed. (Springer, New York, 2007), pp. 178–200.
[26]J. E. Quijano, S. E. Dosso, J. Dettmer, L. M. Zurk, M. Siderius, and C. Harrison, "Bayesian geoacoustic inversion using wind-driven ambient noise," J. Acoust. Soc. Am. **131**, 2658–2667 (2012).
[27]C. J. Geyer, "Markov chain Monte Carlo maximum likelihood," in *Computing Science and Statistics: Proceedings of the 23rd Symposium on the Interface* (Interface Foundation, Fairfax Station, VA, 1991), pp. 156–163.
[28]A. Jasra, D. A. Stephens, and C. Holmes, "Population-based reversible jump Markov chain Monte Carlo," Biometrika **94**, 787–807 (2007).
[29]J. Dettmer and S. E. Dosso, "Trans-dimensional matched-field geoacoustic inversion with hierarchical error models and interacting Markov chains," J. Acoust. Soc. Am. **132**, 2239–2250 (2012).
[30]S. E. Dosso, C. W. Holland, and M. Sambridge, "Parallel tempering for strongly nonlinear geoacoustic inversion," J. Acoust. Soc. Am. **132**, 3030–3040 (2012).
[31]S. Dosso and M. Wilmut, "Uncertainty estimation in simultaneous Bayesian tracking and environmental inversion," J. Acoust. Soc. Am. **124**, 82–97 (2008).
[32]J. Bonnel, S. E. Dosso, and N. R. Chapman, "Bayesian geoacoustic inversion of single hydrophone light bulb data using warping dispersion analysis," J. Acoust. Soc. Am. **134**, 120–130 (2013).
[33]C. F. Mecklenbräuker and P. Gerstoft, "Objective functions for ocean acoustic inversion derived by likelihood methods," J. Comput. Acoust. **8**, 259–270 (2000).
[34]G. Steininger, "Determination of seabed acoustic scattering properties by trans-dimensional Bayesian inversion," Ph.D. thesis, School of Earth and Ocean Sciences, University of Victoria, Victoria, BC, 2013.
[35]T. J. Weingartner, "Vessel collected CTD, NE Chukchi Sea 2008-2013 (Ed5)" (2013), URL https://workspace.aoos.org/group/6316/project/6626/folder/6634/, Alaska Ocean Observing System, Ocean Workspace (Last accessed 2/12/2015).
[36]T. Weingartner, E. Dobbins, S. Danielson, P. Winsor, R. Potter, and H. Statscewich, "Hydrographic variability over the northeast Chukchi Sea shelf in summer-fall 2008-2010," Cont. Shelf Res. **67**, 5–22 (2013).